Validation of the PICIN solver for 2D coastal flows

Qiang Chen[a,*], David M. Kelly[b], Aggelos S. Dimakopoulos[c], Jun Zang[a]

[a] *Research Unit for Water, Environment and Infrastructure Resilience (WEIR), Department of Architecture and Civil Engineering, University of Bath, BA2 7AY, U.K.*
[b] *Coastal Research Lab., International Hurricane Research Center, Florida International University, Miami, Florida, 33199, U.S.A.*
[c] *H R Wallingford, Wallingford, Oxon, OX10 8BA, U.K.*

Abstract

A recent paper Kelly et al. (2015) [SIAM Journal on Scientific Computing 37 (3), B403–B424.] detailed a full particle Particle–In–Cell solver for incompressible free surface flows with two–way fluid–structure interaction called PICIN. In this paper, a 2D version of the method is adapted for simulating the flows encountered in the vicinity of coastal structures. Wave generation and absorption techniques within the hybrid Eulerian–Lagrangian framework used by PICIN are developed for this purpose. The PICIN model is validated against data from three benchmark experiments: i) wave shoaling over a submerged bar, ii) wave overtopping of a Low Crested Structure (LCS) and iii) dam–break induced overtopping of a containment dike. A realistic engineering scenario is also presented that demonstrates the modelling of two–way fluid–structure interaction. The validation study demonstrates that the PICIN model is able to simulate the significant flow processes occurring during wave propagation and transformation, wave impact, overtopping and two–way fluid structure interaction, using relatively little computational resource.

Keywords: Computational Fluid Dynamics, Navier Stokes, Particle–In–Cell, SPH, Incompressible Fluid, Fluid structure interaction

1. Introduction

Within the coastal engineering community, the topic of wave structure interaction which includes, amongst other things, wave generation and absorption, wave slamming, green water overtopping and floating structures has been widely studied both experimentally and numerically (Faltinsen et al., 2004; Chen et al., 2014b; Gao and Zang, 2014; Oliveira et al., 2012; Zhao and Hu, 2012). Due to the continuous increase in computational power over the last few decades numerical CFD models have become increasingly popular

*Corresponding author
Email addresses: Q.Chen@bath.ac.uk (Qiang Chen), dakelly@fiu.edu (David M. Kelly), A.Dimakopoulos@hrwallingford.com (Aggelos S. Dimakopoulos), j.zang@bath.ac.uk (Jun Zang)

in the coastal engineering field as a very efficient tool for physical process understanding and structure optimization (e.g. Richardson et al. (2013)). The Eulerian Volume of Fluid (VOF) based solver interFoam, from the open–source OpenFOAM® modelling suite, has become a very popular numerical tool for investigations in this area. Jacobsen et al. (2012) implemented wave generation and absorption in interFOAM using the wave relaxation zone concept and used the resulting code to investigate wave propagation and breaking. Higuera et al. (2013a,b) developed and validated their OpenFOAM® tool for realistic wave generation and active absorption. Both models show a good agreement with experimental and other numerical data in terms of coastal engineering processes of wave breaking, run up and undertow currents. Chen et al. (2014b) enhanced the OpenFOAM® modules used for wave generation and absorption and subsequently investigated extreme wave interaction with a vertical cylinder. Using this model Chen et al. (2014a) further investigated wave interaction with one degree of freedom 2D box roll motion. Gao and Zang (2014) solved the Reynolds–averaged Navier–Stokes (RANS) equations with $k-\omega$ turbulence model using OpenFOAM® in order to study different kinds of wave impact on a vertical wall.

In terms of meshless (pure) Lagrangian methods for coastal engineering, the Smoothed Particle Hydrodynamics (SPH) method has become very popular and successful during the past decade. Oger et al. (2006) studied a rigid body impacting a water surface, and thus demonstrated the ability of SPH to capture the large pressure variation observed during the impact. Rogers et al. (2010) applied the SPH approach to an engineering problem involving caisson breakwater movement; their results agree relatively well with the experimental data. Bouscasse et al. (2013) developed a SPH scheme for nonlinear interaction between a solid and floating body. In their paper they describe a fully coupled fluid–solid interaction algorithm and validate it by successfully modelling wave packet action on a 2D floating box. Other particle methods for coastal applications have also been developed: Koshizuka et al. (1998) used the Moving Particle semi–implicit (MPS) method to study wave breaking and its interaction with a floating body; Oñate et al. (2008) employed the Particle Finite Element method (PFEM) to investigate fluid–multibody interaction, submerged bodies and bed erosion; Oliveira et al. (2012) adopted the PFEM to study wave overtopping problems with an emphasis on low crest structures.

Hybrid Eulerian–Lagrangian methods are attractive for the use in coastal engineering problems as they combine the efficiency of pure Eulerian methods and the flexibility of pure Lagrangian methods. The arbitrary Lagrangian–Eulerian (ALE) model was first introduced to fluid dynamics problems by Hirt et al. (1974), where a methodology based on a movable finite difference mesh was presented. Ramaswamy (1990) developed an ALE model for incompressible viscous free surface flows based on the finite element method.

Zhou and Stansby (1999) developed an ALE model in the σ coordinate system for shallow water flows and enhanced this model to accommodate a vertically moving mesh; their model shows good results for simulating wave behaviour over bars. In this paper, we present the validation of another hybrid Eulerian–Lagrangian model PICIN (Kelly et al., 2015) for coastal engineering problems.

The PICIN model is a full particle Particle–In–Cell solver (e.g. Brackbill and Ruppel (1986); Zhu and Bridson (2005); Kelly (2012)) for incompressible free surface flows. The model handles two–way fluid structure interaction using the Distributed Lagrange Multiplier (DLM) method introduced by Patankar et al. (2000); as such, the technique can handle floating and sinking bodies as well as mobile structures such as caisson breakwaters and wave energy devices. As a hybrid method, the PICIN code has all the advantages of a Lagrangian approach with the efficiency of an Eulerian approach. The model can simulate the severe free surface deformation associated with overturning waves and violent impacts. Moreover, the DLM method allows for multiple interacting solid bodies within the computational domain with a relatively small computational overhead (Chen et al., 2015a). For application to wave–structure problems, a numerical wave tank (NWT) has been established in PICIN thus enabling the model with wave generation and absorption capability. In PICIN, waves are generated using a piston wave maker, where the cut–cell type solid boundary described in Kelly et al. (2015) is employed. Wave absorption at the far end of the NWT is implemented using a relaxation technique following Jacobsen et al. (2012).

The paper is organised as follows: section 2 gives an overview of the PICIN model including the governing equations and the numerical solution technique. Next, section 3 details the implementation of a paddle type wave maker and wave absorption zone within the PICIN model framework. In section 4 we compare results of the PICIN model with idealised and more complex real world type test cases. Finally, conclusions are drawn in section 5.

2. The PICIN Model

2.1. Governing equations

The PICIN model is based on the governing equations for two–way coupled fluid–solid motion proposed by Patankar et al. (2000). Within this framework, the computational domain is considered to contain both the fluid and any solid bodies and is denoted by Ω. The fluid and solid domains are subsets of Ω and are denoted by Ω_F and Ω_S respectively. On the boundary of Ω, denoted by $\Gamma = \Gamma(\boldsymbol{x}, t)$, problem specific boundary conditions are enforced (i.e. the wave paddle described in section 3). The system of equations

governing the fluid and solid motion has the following form:

$$\nabla \cdot \boldsymbol{u} \;=\; 0, \tag{1}$$

$$\frac{\partial \boldsymbol{u}}{\partial t} + (\boldsymbol{u} \cdot \nabla)\boldsymbol{u} = \boldsymbol{f} - \frac{1}{\rho}\nabla p + \nu \nabla^2 \boldsymbol{u} \quad \text{in } \Omega_F, \tag{2}$$

and:

$$\frac{\partial \boldsymbol{u}}{\partial t} + (\boldsymbol{u} \cdot \nabla)\boldsymbol{u} = \boldsymbol{f} - \frac{1}{\rho_S}\nabla p + \nabla \cdot \boldsymbol{\Pi} \quad \text{in } \Omega_S. \tag{3}$$

With the following boundary conditions on the free surface and moving solid boundaries respectively:

$$\boldsymbol{u} = \boldsymbol{u}_i \text{ and } p = 0 \quad \text{on } \zeta(\boldsymbol{x}, t), \tag{4}$$

where $\zeta = \zeta(\boldsymbol{x}, t)$ is the free surface and:

$$\boldsymbol{u} = \boldsymbol{u}_i \text{ and } (\boldsymbol{\Pi} - p\boldsymbol{I}) \cdot \hat{n} = \boldsymbol{T} \quad \text{on } \partial\Omega_S(\boldsymbol{x}, t), \tag{5}$$

which implies a no–slip condition on the boundary of Ω_S here denoted as $\partial\Omega_S = \partial\Omega_S(\boldsymbol{x}, t)$. Note that for grid–aligned fixed solid boundaries the free–slip condition can be imposed; for example, the domain boundary denoted by $\partial\Omega_F$ (see Kelly et al. (2015)). In two spatial dimensions $\boldsymbol{u} = [u, w]^T$ is the velocity field, p is pressure, $\boldsymbol{f} = [0.0, -9.81]^T$ represents the vector of body force acting on the water due to gravity, ρ is the water density, ρ_S is the solid density and ν is the kinematic viscosity of water. The traction force of the fluid on the solid, denoted by $\boldsymbol{T}$, is the sum of the projected viscous stresses and pressure. $\boldsymbol{I}$ is the identity tensor. $\boldsymbol{\Pi}$ is defined as an extra stress tensor, in addition to the pressure field p, due to the rigidity constraint (Patankar et al., 2000). Note that instead of solving for $\boldsymbol{\Pi}$ directly, in PICIN the rigidity constraint is implicitly enforced through the approach proposed in Patankar et al. (2000). For full details of the equations solved in the PICIN model the interested reader is referred to Kelly et al. (2015).

2.2. Numerical Solution Procedure

The PICIN model employs the full particle PIC methodology of Brackbill and Ruppel (1986), see also Zhu and Bridson (2005); Kelly (2012); Edwards and Bridson (2012), modified for one– and two–way fluid structure interaction. The approach uses a finite difference form of the governing equations (Eq. 1–Eq. 3) to apply body forces, boundary conditions and the accelerations due to pressure gradients. This stage of the solution procedure is Eulerian in nature and is performed on an underlying staggered Cartesian mesh

(Harlow and Welch, 1965). The non–linear advection term is handled in a Lagrangian sense employing particles in order to reduce numerical diffusion and simplify the handling of the free surface boundary. The numerical method is based on time–operator–splitting which uses pressure as a Lagrange multiplier that enforces a divergence free velocity field (Chorin, 1968). The model is thus hybrid Eulerian–Lagrangian and, as such, handles complex free surface flows whilst achieving a high level of efficiency for the solution of the pressure Poisson equation (PPE). Fixed solid boundaries that do not conform to the simple underlying Cartesian grid are treated via a cut–cell type approach and non–fixed solid boundaries are handled using a modified version of the DLM approach (Patankar et al., 2000; Kelly et al., 2015). For enhanced accuracy, the Dirichlet boundary condition for (zero) pressure is applied directly at the free surface using a signed distance function that is constructed at each time step of computation. Full details of the PICIN solution algorithm can be found in Kelly et al. (2015).

3. Wave generation and absorption

3.1. Numerical Wave Paddle

In this paper, certain test cases require the generation and absorption of gravity waves. Accurate wave generation is essential if the model results are to be meaningful. There are a variety of techniques that can be used to generate a wave train including the internal wave maker (source term) approach (Lin and Liu, 1999), the relaxation zone approach (Engsig-Karup et al., 2006; Jacobsen et al., 2012), the boundary condition approach (Higuera et al., 2013a; Chen et al., 2014b) and the wave paddle approach (Ursell et al., 1960; Oliveira et al., 2012). In this paper we employ a moving paddle approach to generate waves. Following Oliveira et al. (2012) the variation of the paddle location in time is obtained via first–order wave maker theory and the displacement is prescribed simply as $X(t) = \int_0^t u(t)\,\mathrm{d}t$. The paddle velocity is prescribed as:

$$u(t) = \frac{H}{2C}\omega\cos\omega t \tag{6}$$

where:

$$C = \frac{4\sinh^2 k_0 h}{2k_0 h + \sinh 2k_0 h}, \tag{7}$$

here H, ω and k_0 represent the target wave height, wave frequency and wave number respectively and h accounts for the water depth. A validation of wave generation capability of PICIN is presented in Appendix A. For the test case in subsection 4.3 wave ramping is required to alleviate the transients typically associated

with impulsive starting and stopping of the paddle, the paddle displacement X_R is prescribed as:

$$X_R(t) = \begin{cases} X(t)\frac{t}{T} & 0 < t \leq T \\ X(t) & T < t \leq NT \\ X(t)(1 - \frac{t-NT}{T}) & NT < t \leq (N+1)T \end{cases} \tag{8}$$

with N being the desired number of waves, which is set to 3 for the test case in subsection 4.3.

At each time step the boundary condition for the wave paddle in PICIN is implemented as a fixed solid boundary with a given velocity. The cut–cell approach described in Kelly et al. (2015) is used when the paddle is not aligned with the grid. It should be noted that the numerical wave paddle implemented in the current version of PICIN does not provide active absorption.

3.2. Absorption

Wave absorption at the downstream end of the numerical flume is achieved via a relaxation zone following Jacobsen et al. (2012). The relaxation approach is straightforward to implement in PICIN. After the advection step, velocities in part of the computational domain are forced according to the desired analytical solution $\boldsymbol{u}_a$, which in our case is water at rest i.e. $\boldsymbol{u}_a = [0, 0]^T$, as we are only interested in using the relaxation approach for absorption. The relaxation zone used for absorption in this paper is two wave lengths long unless stated otherwise. With the desired analytical velocity denotes by $\boldsymbol{u}_a$ and the computed numerical velocities denoted by $\boldsymbol{u}_n$ the equation used to determine the relaxation velocities is:

$$\boldsymbol{u}_r = R(x)\boldsymbol{u}_a + (1 - R(x))\boldsymbol{u}_n. \tag{9}$$

The relaxation coefficient is a function of horizontal location $R = R(x)$ having a value of zero at the start of the absorption zone and ramping up to unity at the downstream end of the computational domain. When implementing this approach in PICIN, we force the particle velocities to the relaxation velocities at the end of each time step after the numerical solution is found. Additionally, in the relaxation zone the PICIN model reverts from a weighted average of full particle PIC (Brackbill and Ruppel, 1986) to pure classical PIC (Harlow, 1964). The large numerical diffusion inherent in the classical PIC approach acts to further damp the waves. Validation of the wave absorption method is given in Appendix A.

4. Validation Tests

In this section, a number of test cases are presented in which the PICIN model is validated against experimental data as well as results from other state–of–the–art numerical models. Emphasis is given to the validation of the model for hydrodynamic processes occurring in the vicinity of coastal structures, such as: wave propagation and shoaling, prediction of overtopping volumes and wave forces obtained from impact pressures. Four benchmark cases are used to demonstrate the capability of PICIN to successfully simulate such problems, these are: i) Shoaling over a submerged bar (Ohyama et al., 1995), ii) Flow over a containment dike (Greenspan and Young, 1978), iii) Overtopping of a low–crested structure (LCS) (Oliveira et al., 2012), and iv) Wave impact on a mobile caisson breakwater (Wang et al., 2006).

4.1. Shoaling over a submerged bar

This test was used by Ohyama et al. (1995) to determine the applicability of three distinct mathematical models of nonlinear dispersive waves. The authors presented experimental data for various waves propagating over a submerged trapezoidal bar. The configuration of the flume bathymetry in the physical and the numerical model is illustrated in Fig. 1, where the characteristic dimensions and the location of the free-surface elevation probes are shown. In the physical model, six wave conditions were tested, emerging from the combination of three wave periods with two wave heights. For the PICIN model, only the larger wave height is considered ($H_0/h_0 = 0.1$), resulting in a total of three wave conditions, namely Cases 2 , 4 and 6 in Ohyama et al. (1995) with wave periods $T_0\sqrt{g/h_0}$=5.94, 8.91 and 11.88, respectively. In the physical model a piston type wave maker was used to generate the waves and a wave absorber is used to remove wave reflection at the end of the flume. The physical wave tank is 65 m long, 1.0 m wide and 1.6 m high and the water depth h_0 was set to 0.5 m. The distance from the centre of the submerged bar to the wave maker was 28.3 m.

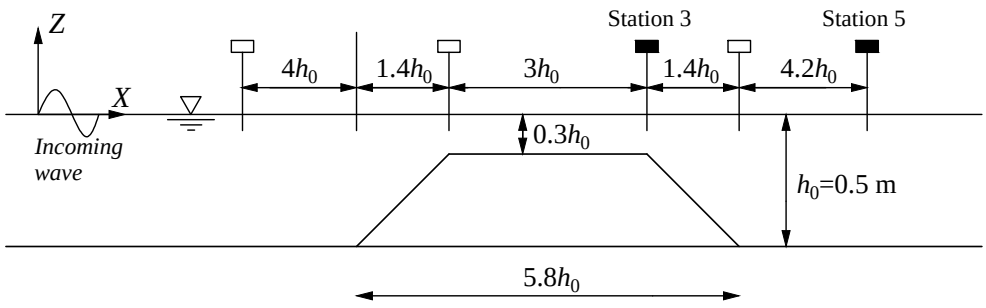

Fig. 1: Schematic showing the initial conditions and wave gauge locations for Test 1.

In the PICIN model, while the distance from the centre of the submerged bar to the wave maker was nearly the same as that used in the experiment (28.45 m), the overall length of the NWT was set to 48 m, 53 m and 58 m for Cases 2, 4 and 6 respectively, in order to reduce the CPU cost. The wave absorption zone at the end of the NWT was at least three wave lengths long for all cases. The mesh size was set to 0.01 m $\times$ 0.01 m, resulting to, for example, a cell resolution of 5300 $\times$ 76 with a total number of around 1 million particles for case 4. The simulation was run by setting the maximum Courant number to 0.5 and the run–time was, for instance, approximately 14.4 hours for 50 s of simulation time for case 4, in serial execution (core specification: Intel(R) i5–3470 CPU @3.2GHz). In the numerical simulations the water density is set to 1000 kgm^{-3} and the dynamic viscosity is set to $\mu = 1.0 \times 10^{-3}$ kgm^{-1}s^{-1}; these values were used for all the test cases in this paper. Free-surface elevation snapshots showing the evolution of the waves and the vertical velocity distribution are presented in Fig. 2 for Case 4, where the nonlinear interaction of the waves with the submerged bar is demonstrated.

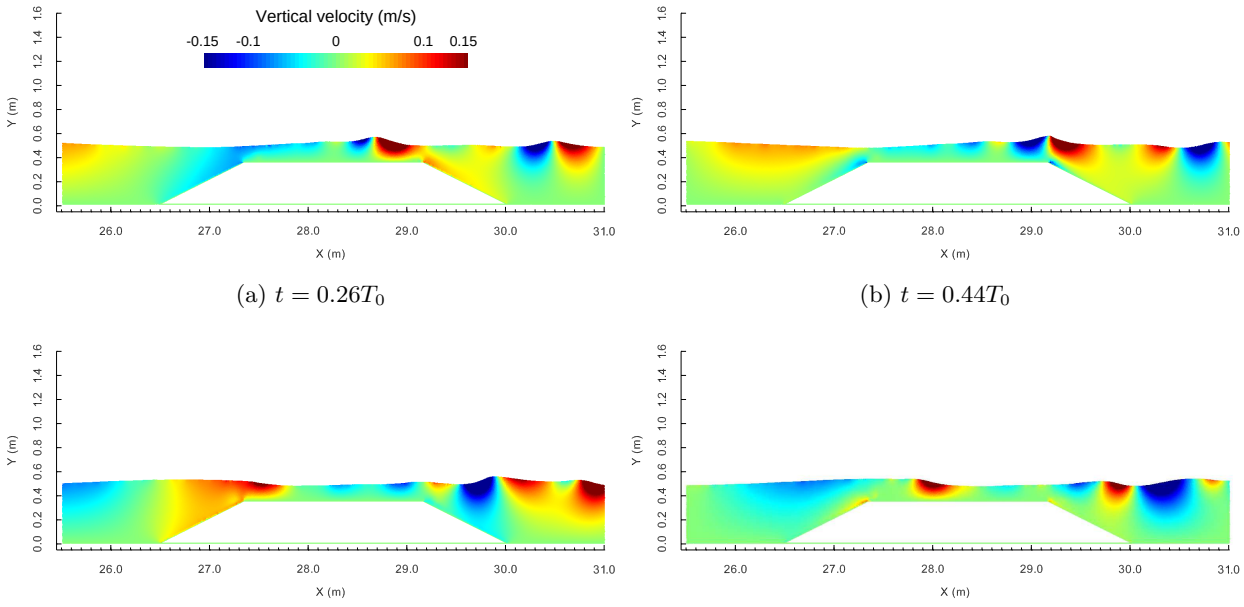

(a) $t = 0.26T_0$ (b) $t = 0.44T_0$

(c) $t = 0.71T_0$ (d) $t = 0.93T_0$

Fig. 2: Close–up snapshot of wave profile with vertical velocity field in the immediate vicinity of the trapezoidal submerged bar for case 4.

Comparison of numerical predictions from the PICIN model and the fully nonlinear model (digitised from Ohyama et al. (1995)) and experimental data of free surface evolution in time at Stations 3 and 5 (see Fig. 1) are given in Fig. 3. Note a time shift has been used in order to match the phase at station 3 for all cases when presenting the PICIN results. It is noted that when compared with the experimental data,

the PICIN results generally agree better at station 3 than at station 5; this is further confirmed by the root mean square errors (RMSE), which are around 7% and 25% for all cases at Stations 3 and 5, respectively. The relatively high RMSE at station 5 is primarily due to the phase error, which is likely to be caused by the lack of resolution for the decomposed high–order harmonics when they propagate into the shoreward region. For the wave elevation at station 5 of Case 2, where the waves are steeper and almost reach the breaking limit, the PICIN model does not give very good results. This could be caused by the increased numerical diffusion due to high wave steepness and closeness to breaking incipient. Nevertheless, it is demonstrated through all cases that PICIN is inherently capable of modelling fully non-linear waves as the shape of wave forms are captured correctly. This is a solid indication that the numerical methodology and the innovative treatment of the nonlinear advection terms through particle advection is capable of modelling fully nonlinear wave dynamics.

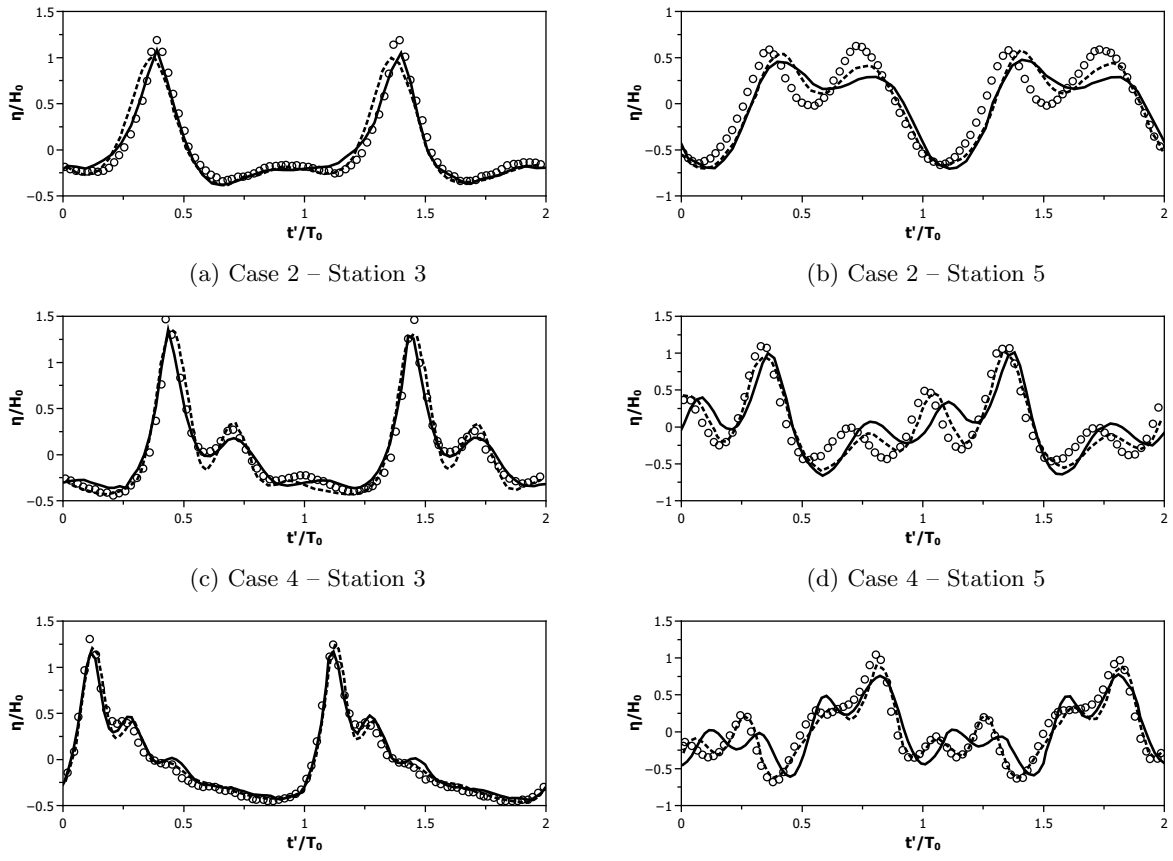

(a) Case 2 – Station 3

(b) Case 2 – Station 5

(c) Case 4 – Station 3

(d) Case 4 – Station 5

(e) Case 6 – Station 3

(f) Case 6 – Station 5

Fig. 3: Comparison of PICIN predictions (solid lines), fully nonlinear model results from Ohyama et al. (1995) (dashed line) and experimental data (circles) for free surface elevations at Stations 3 and 5 of experiment Cases 2, 4 and 6.

4.2. Flow over a containment dike

This test demonstrates the capability of PICIN to cope with violent impacts and overtopping. The model results are compared with the experimental measurements presented in Greenspan and Young (1978) for dam break flow impacting a containment dike. The initial conditions of the physical model are shown in Fig. 4.

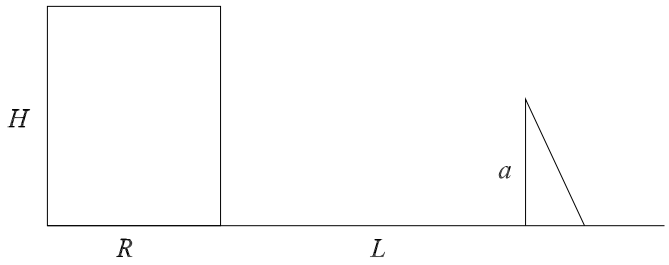

Fig. 4: Flow over a containment dike: Experiment set-up

Seven simulation cases were set–up for the PICIN model. The height of the dike, a, width of the water column, R, and the distance from the water column front to the dike, L, were kept constant (0.5 m, 1.0 m and 1.0 m, respectively), while the height of the water column H was set to the following values for each case (in metres): 0.45, 0.5, 0.65, 0.8, 1.1, 1.4, 1.55. The cell size is set to 0.01 m ($a/100$) for all simulations, while the geometry for each case is slightly different, as for the cases initiating with higher water columns, an appropriate extension of the top and right hand side boundary is needed, to cover the areas of important flow dynamics. The mesh size ranges from $120,000$ cells to $420,000$ cells and four particles per cell were seeded initially. The time–step control is achieved by setting the maximum Courant number at 0.5 and the duration of each simulation is adjusted to correspond to the corresponding experiment (around a second).

Snapshots of the free surface evolution for seven time frames are shown in Fig. 5. The time frames are selected so as to provide a direct comparison with the video sequence shown in Figure 8 of Greenspan and Young (1978). It is observed that as the water column collapses, the leading water front moves faster than the rest of the water and collides with the dike, resulting in an extremely violent impact. This impact causes a thin 'spike' of water to bounce violently skywards, a phenomenon which clearly indicates the development of impulsive pressure. The bulk of the water that follows the leading front accumulates behind the dike and subsequently overtops the dike, by forming a distinctive round overtopping jet. Both the spike and the overtopping jet are pulled downwards by gravity, once they overtop the dike. The bulk flow evolution and the development of secondary features are well captured by the PICIN model, as confirmed by the direct comparison of the numerical and the physical model snapshots, in the sequence presented in Figure 8 of

Greenspan and Young (1978). There are some differences observed in the evolution of the vertical spike of water as in the numerical model, this secondary feature evolves as a thin coherent jet that reaches higher than in the physical model (a phenomenon also observed in the numerical model results of Johnson et al. (1994)), while in the latter, the jet breaks up to form multiple spikes. This is most likely because the PICIN model does not include aeration and surface tension effects and these effects play an important role in shaping small–scale features in two phase flows. In addition, discrepancies with respect to the dimensionless time interval (we use dimensionless time here as we employ metres for the dimensions in the numerical simulation as opposed to inches in the experiments) between snapshots are shown. The predicted position of the water front evolves more quickly (i.e. there is a smaller time interval between the snapshots) than that of the experiment during the impact (Fig. 5(a)-(c)), but the predicted evolution is slightly slower than the experiment afterwards (Fig. 5(c)-(f)). The faster motion of the flow during the impact is likely due to the lack of air resistance, surface tension and bed friction in the numerical model and, as a result of these factors, a larger proportion of the bulk water body bounces up, which causes the delay as gravity pulls the water jet downwards (hence the larger time interval between the snapshots in the numerical simulation).

The volume of water that overtopped the dike at the end of the experiment was measured both at the physical and the numerical models. The spillage fraction is derived as the ratio of the overtopped volume over the total and the variation of the spillage fraction as a function of a/H is presented in Fig. 6 in comparison with the experimental data. It is observed that the PICIN model individually captures some of the overtopping values with high precision and predicts the trend of overtopping fluxes particularly well. The RMSE of the B–spline trend, normalised to the maximum flux, is 2.8%.

4.3. Overtopping of a Low Crested Structure (LCS)

In Oliveira et al. (2012), a physical model of wave overtopping for regular non–breaking waves over a simple, low–crested, impermeable maritime structure is presented and results are used to validate the Particle Finite Element Method (PFEM)(Oñate et al., 2004). The experiment was performed at the Maritime Engineering Laboratory of UPC–BarcelonaTech, in a wave flume 18 m long, 0.4 m wide, and 0.6 m deep, using a piston–type paddle to generate the regular waves. More details on the modelling procedure can be found in Oliveira et al. (2012). The initial conditions used for the experiments and the numerical simulations are shown in Fig. 7, along with the location of the free-surface elevation probes. In the physical model, two cases were tested corresponding to a group of four regular waves with period $T = 1.55$ s and wave heights of $H = 0.06$ m and $H = 0.07$ m, respectively. In both cases, the first and the last wave were linearly ramped

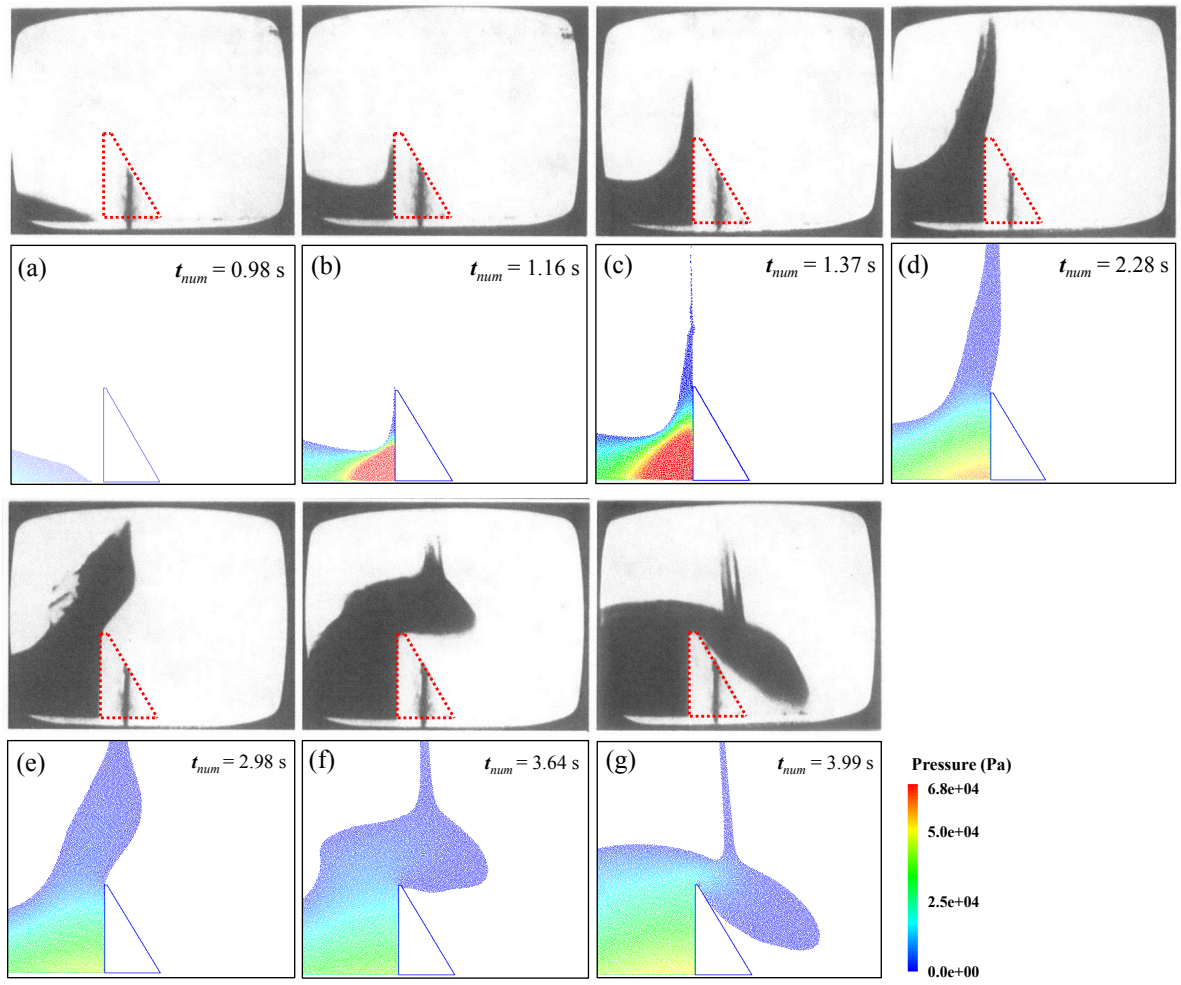

Fig. 5: Above: Experimental photos of Greenspan and Young (1978), rearranged and modified to include the dike location, reproduced with the kind permission of Cambridge University Press and Professor H. P. Greenspan. Below: Snapshots of PICIN model results at the flow status similar to that of the photographs. In the numerical simulation, H = 8 m, R = 9 m, L = 9 m and a = 4 m. The time intervals, normalised by $\sqrt{a/g}$, correspond to approximately 0.69 in the experiment, and 0.28 (a–b), 0.33(b–c), 1.43(c–d), 1.10(d–e), 1.03(e–f) and 0.55 (f–g) in the numerical modelling.

and the two middle waves were generated at full height. The wave generation set-up is replicated at the PICIN model for the lower wave height case (H = 0.06 m).

The mesh is generated using about 35000 cells of 0.01 m × 0.01 m size and about 65000 particles. The simulation was run for 20 s (Courant number = 0.5) and required around 40 minutes of CPU time using an Intel(R) i5-3470 CPU @3.2GHz core. The PICIN model is, in this test case, thus significantly more efficient than the PFEM model of Oliveira et al. (2012) as the latter required 50 hours of CPU time on a 2.67GHz Intel Core i7 CPU920.

Four snapshots of the flow field are shown in Fig. 8 during run–up and run–down of the second wave at the low–crested structure, where the horizontal velocity field is also illustrated. It is noted that the PICIN

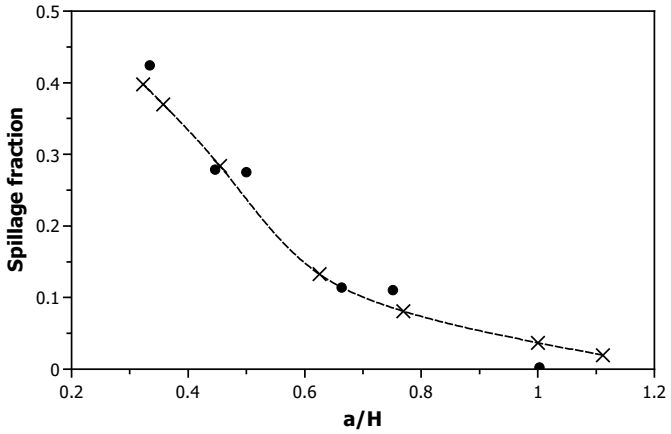

Fig. 6: Overtopping fluxes against a/H: Filled circles correspond to the physical model data while $\times$ symbol to numerical model predictions. The dashed line is the B–spline trend of numerical data.

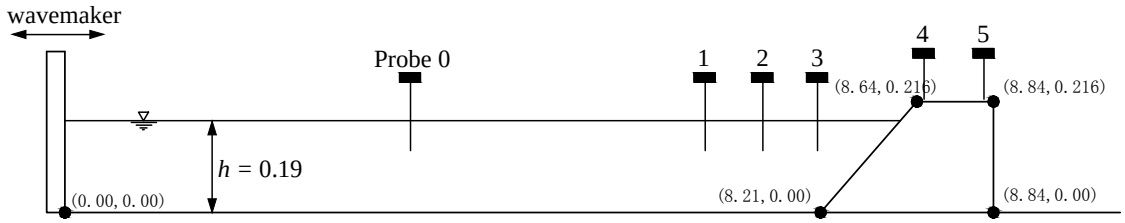

Fig. 7: Schematic showing the initial conditions and wave gauge locations for test 3; all dimensions in (m).

model predicts wave run–up and overtopping naturally obviating the need for an explicit (and often involved) shoreline treatment. The velocity field provides some further insights on the overtopping jet evolution such as the jet reversal during run-down, which hints that not all the water volume rising above the water level eventually overtops the structure.

Quantitative comparisons for wave transformation and wave overtopping are shown in Fig. 9, where PICIN predictions are compared with those obtained in the UPC flume. It can be seen that good agreement has been achieved between the PICIN results and the experimental observations in Oliveira et al. (2012). From the first four panels (a)–(d) in Fig. 9 (wave probes 0–3, Fig. 7), it is evident that the PICIN model reproduces with high fidelity the wave generation in the experiment and accurately predicts the nonlinear effects of wave generation, wave propagation, and wave transformation induced by the LCS.

The free–surface elevation recorded at the last two panels (e) and (f) of Fig. 9 (wave probes 4 and 5, Fig. 7) corresponds to the thickness of the overtopping jet. In general, it is observed that the numerical model predicts the overtopping jet evolution very well. At Fig. 9(e), there is a slight overprediction of the peak values from the numerical model, which is probably due to processes that can cause a mild reduction

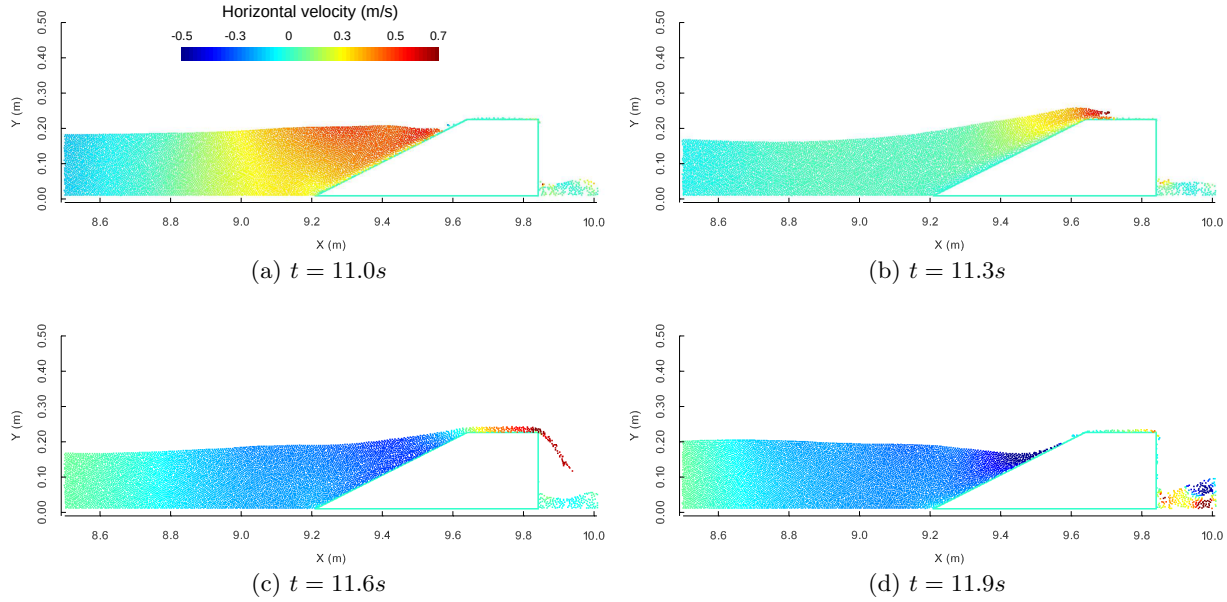

(a) $t = 11.0s$ (b) $t = 11.3s$

(c) $t = 11.6s$ (d) $t = 11.9s$

Fig. 8: Close–up of wave profile and horizontal velocity field near the LCS during overtopping for the second main wave train.

of wave run–up over smooth slopes and not included in the numerical model, such as air resistance and turbulence. A slight phase delay can also be observed, especially for the first and last overtopping peaks, which is probably due to the lack of resolution in the simulations where the thin layer of water on the top of LCS is not well resolved. During transition from the front to the back of the LCS crest, the numerical model predicts a decrease of the overtopping jet thickness, which is well–known behaviour (Pullen et al., 2007).

4.4. Wave impact on a mobile caisson breakwater

The final test in this paper concerns the modelling of two–way wave structure interaction during the wave loading of a caisson breakwater. The test is based on the experiments conducted by Wang et al. (2006) and was used by Rogers et al. (2010) in order to validate the SPHysics SPH solver for two–way fluid structure interaction. Initial conditions of the experiment and the numerical simulation are shown in Fig. 10. Following Wang et al. (2006) a piston–type wavemaker was used to generate waves with a period of 1.3 s and a wave height of 0.167 m at the paddle. In their SPHysics simulation Rogers et al. (2010) placed a 1:10 beach shoreward of the caisson to dissipate any wave motion generated by the moving block. For the PICIN model, the relaxation approach for wave absorption is adopted for the same purpose. As in Rogers et al. (2010), the rubble mound under the caisson is treated as an impermeable structure. This is because PICIN does not yet have the capability to model sub–grid porous flow, i.e. by using the Volume Averaged

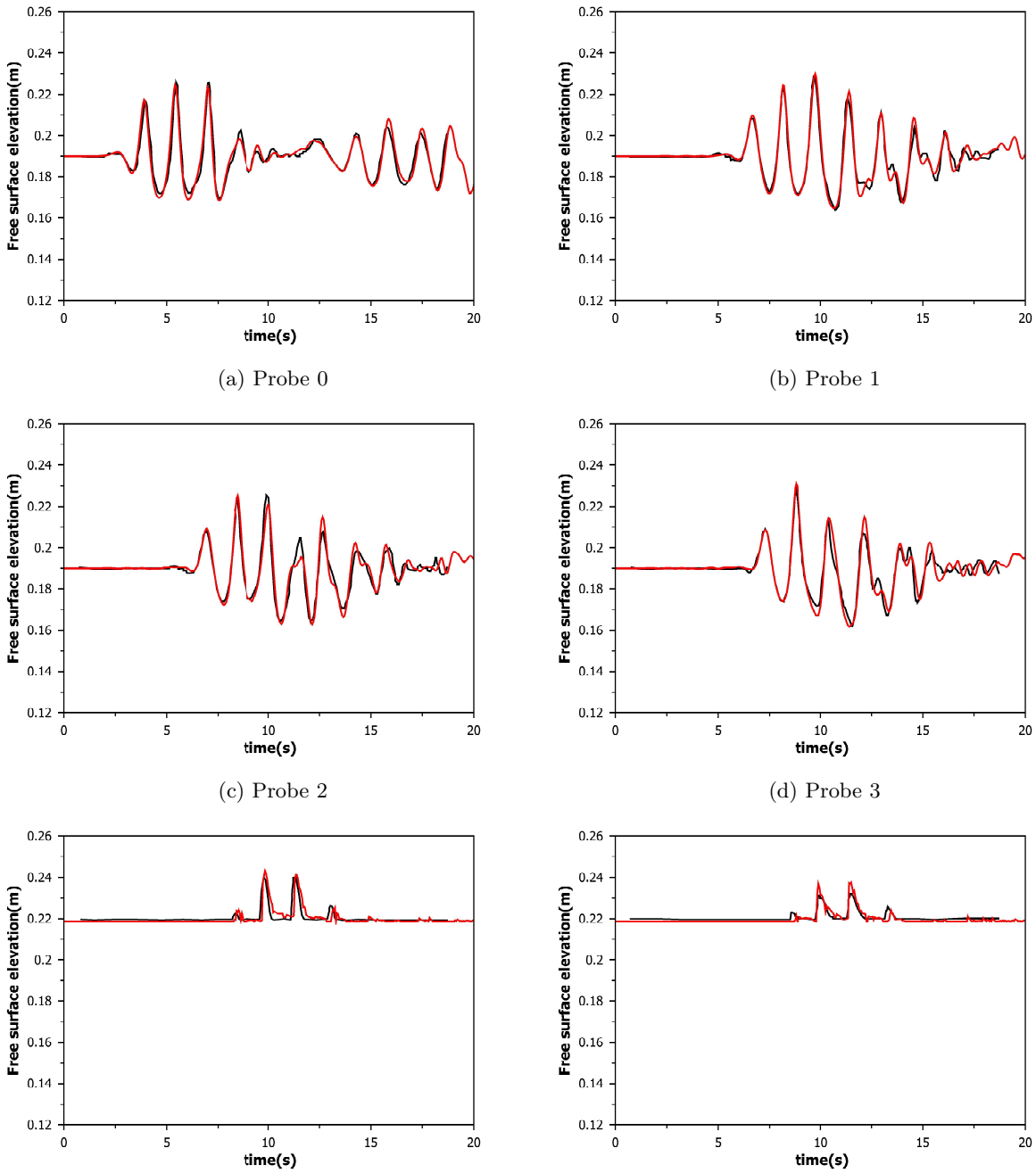

(a) Probe 0

(b) Probe 1

(c) Probe 2

(d) Probe 3

(e) Probe 4

(f) Probe 5

Fig. 9: Comparison of PICIN predictions (red lines) and experimental data (black lines) for free surface elevation at the six wave probes in test 3.

Navier-Stokes equations described in Hsu et al. (2002).

The caisson breakwater is allowed to move horizontally and a friction force between the caisson and the rubble mound is applied. Following Rogers et al. (2010), a threshold velocity value of the caisson is used to

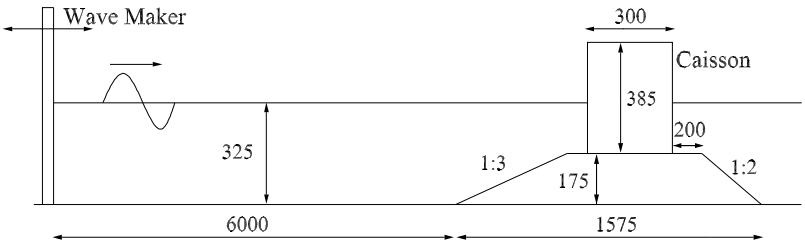

Fig. 10: Numerical model set-up for the caisson breakwater test case of Wang et al. (2006); all dimensions in (mm)

detect whether static or dynamic friction force should be used as a resistance to the motion of caisson due to wave interaction. Based on this idea, the friction force is expressed as:

$$f_{\text{friction}} = \begin{cases} \min(f_{\text{dynamic}}, f_{\text{static}}) & \text{if } \|\boldsymbol{v}_t\| \leq \|\boldsymbol{v}_{t,\text{threshold}}\| \\ \min(f_{\text{dynamic}}, f_{SD}) & \text{if } \|\boldsymbol{v}_{t,\text{threshold}}\| < \|\boldsymbol{v}_t\| \leq 2\|\boldsymbol{v}_{t,\text{threshold}}\| \\ f_{\text{dynamic}} & \text{if } \|\boldsymbol{v}_t\| > 2\|\boldsymbol{v}_{t,\text{threshold}}\| \end{cases}, \tag{10}$$

where

$$f_{SD} = f_{\text{static}} + \left(\frac{\|\boldsymbol{v}_t\|}{\|\boldsymbol{v}_{t,\text{threshold}}\|} - 1 \right) (f_{\text{dynamic}} - f_{\text{static}}), \tag{11}$$

here $\boldsymbol{v}_{t,\text{threshold}}$ and $\boldsymbol{v}_t$ are the threshold velocity and caisson velocity, respectively; f_{static} and f_{dynamic} represent the static and dynamic fiction force from the foundation, respectively. In PICIN, f_{static} was set equal to the wave force at each time step and f_{dynamic} was calculated by multiplying the caisson weight and a friction coefficient $\mu = 0.5$ given by Rogers et al. (2010). f_{SD} is simply a transition force linearly interpolated between the static and dynamic forces.

The simulations presented here used the mesh size $\Delta x = \Delta z = 0.013$ m. A Courant number of 0.5 was employed to determine the adaptive time step. The simulation takes 1.44 hours to complete at an Intel(R) i5-3470 CPU @3.2GHz core, for 15 s of simulation time. The computational requirements are relatively small; however, the computational requirements for the SPHysics model are not given in Rogers et al. (2010) for comparison.

In Fig. 11 snapshots of the wave–caisson interaction predicted by the PICIN model (right panel, Fig. 11) are compared with those of the SPHysics model presented in Rogers et al. (2010) (left panel, Fig. 11). In these snapshots, it is observed that as the waves reach the toe of the structure, they form a high-steepness front as they shoal up, which indicates wave breaking initiation. As the incident wave interacts with the

structure, the following processes occur, i) wave reflection ii) wave overtopping and iii) structure motion due to the dynamic loading. All three processes are predicted by the numerical model thus showing that PICIN has the potential to model the key processes which are critical for the design of coastal structures. The free–surface evolution and the pressure distribution are also qualitatively and quantitatively very similar to those presented in Rogers et al. (2010).

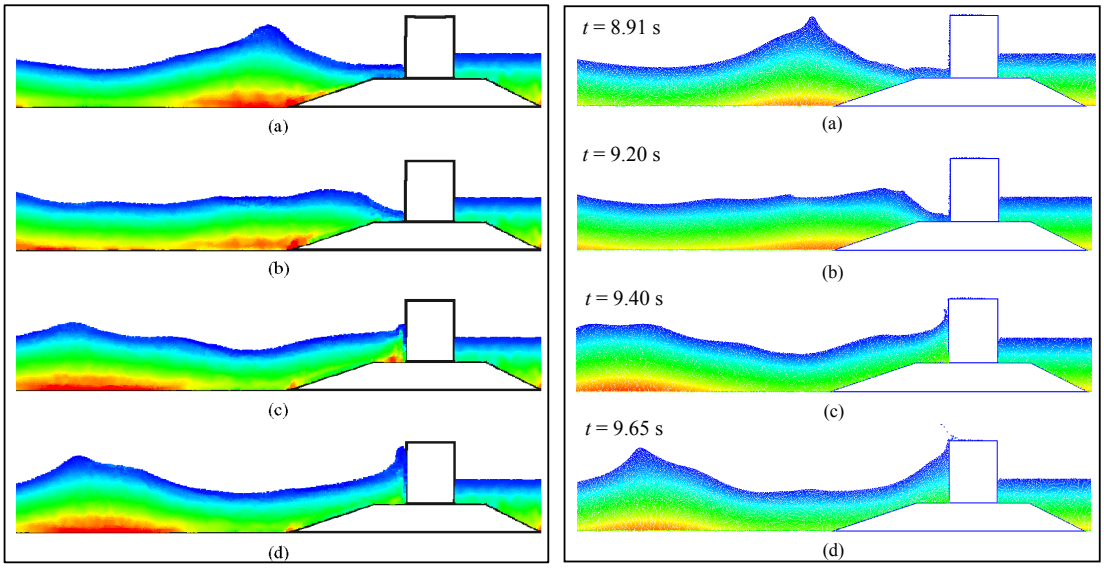

Fig. 11: Snapshots of the PICIN simulation results (right panel) at flow configurations similar to those presented in snapshots of the SPHysics model results (left panel[1]) for wave and caisson interactions. The pressure fields p in both panels are visualised with contour colours scaled from 0 kPa (blue) to 4 kPa (red).

The comparisons between experimental data and numerical results for the overall horizontal wave force and caisson movement are shown in Fig. 12. In this paper, the wave force is compared when the numerical model reached a fully developed state, while the caisson displacement was considered when the caisson started to move backward after a slight forward motion due to the water level change. In order to check the robustness of the methodology proposed in Eq. 10 and Eq. 11, two values of threshold velocities were used in PICIN, 0.001 m/s and 0.002 m/s, respectively. Both the experimental data and the results of the SPHysics model are digitised from the plots presented in Rogers et al. (2010).

In Fig. 12(upper panel), it is observed that the quasi-static horizontal wave force component is relatively well captured by both models, in terms of both shape and amplitude. For the PICIN model, the impulsive part of the wave forces is not as well captured, but this is to some level expected. As stated before, PICIN

[1]reproduced from Rogers et al. (2010), copyright©International Association for Hydro–Environment Engineering and Research, by permission of Taylor & Francis Ltd, www.tandfonline.com on behalf of International Association for Hydro–Environment Engineering and Research.

does not include aeration effects, which play a crucial role in the evolution of the wave force peaks through air bubble entrapment and air compression at the breaking wave front (Cuomo et al., 2010). The change in the threshold velocity has a considerable impact on the impulsive peaks but a less significant one on the quasi–static component of the wave loading. There is also a phase difference observed after 5 s between the results from PICIN model and experimental data, and this may be due to differences in the structure response in the numerical and the physical models.

In Fig. 12(lower panel), the cumulative displacement of the caisson is presented for both the physical and the numerical models. The physical model results show that the caisson is pushed back and forth by the waves with a slight landward drift. The response period of the motion is equal to the wave period and it is well predicted by both the PICIN model and SPHysics model. The overall trend of the displacement is also well captured by the numerical models and compares well with the experimental data. From the PICIN results, it can be seen that using threshold velocity 0.002 m/s gives larger overall displacement up to $t \sim 3$ s and similar later on. More significant differences are observed in the evolution of the displacement, rather than the overall values. In the physical model the evolution is practically stepwise, consisting of sudden landward motions and relatively smooth seaward motions. The evolution of the numerical model resembles a harmonic motion with a smooth increase of the mean level, rather than a stepwise progression. It is also observed from the PICIN results that changing the value of the threshold velocity does not seem to improve the caisson response. A similar difference is also observed from the SPHysics model results. Herein, we argue that this is because the porous pressures acting at the foundation of the caisson are not included both in PICIN and SPHysics. The inclusion of these pressures would change the response significantly, as, during wave impact, the peak dynamic pressures would push the caisson upwards, lowering the friction force significantly or even instantaneously lifting up the caisson. This could explain also the fact that the stepwise progression of the caisson is synchronised with peaks in the force time series in the experiment (Fig. 12). On the contrary, when negative wave loads act on the structure, negative pressures transmit to the caisson foundation and act to decrease buoyancy, thus making it more difficult to move seawards. In the numerical model, the friction parameters correspond to an average buoyant weight of the caisson and do not include these changes in the apparent weight, caused by the pressure transmission inside the rubble mound. It is therefore argued that modelling the rubble mound as a porous medium will result in the improvement of the results. We note that the PICIN results presented for this test were previously presented at the 30^{th} International Workshop on Water Waves and Floating Bodies (Chen et al., 2015b).

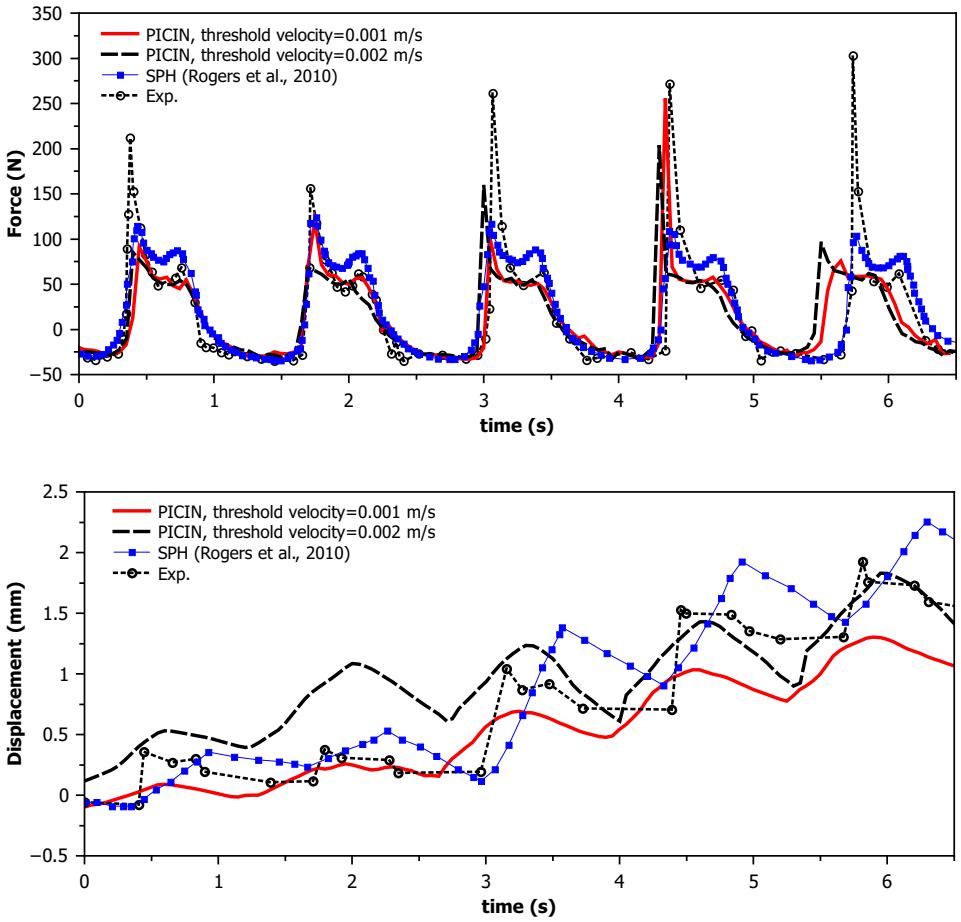

Fig. 12: Comparisons of horizontal wave force (upper panel) and Caisson displacement (lower panel) between results from experiment (digitised from Rogers et al. (2010)), SPHysics and PICIN.

5. Conclusions

This paper assesses the performance of the full particle PIC model, PICIN (Kelly et al., 2015), for coastal engineering applications. In the paper a numerical wave flume is implemented that employs a cut–cell type solid boundary technique for wave generation and a relaxation method for wave absorption. The model is validated against four benchmark cases: nonlinear wave transformation over a submerged bar (Ohyama et al., 1995), wave impact and overtopping of a containment dike(Greenspan and Young, 1978), wave overtopping of a low–crested structure (LCS)(Oliveira et al., 2012), and wave impact and two–way fluid solid interaction with a caisson breakwater (Wang et al., 2006). In all cases, the PICIN model is able to reproduce the key processes well using relatively little computational resource. Moreover, the PICIN model requires no special treatment for predicting nonlinear behaviour and complex phenomena pertaining to wave

propagation, transformation, run–up and overtopping. The PICIN model still requires further developments; in particular, the model would benefit from porous media implementation, inclusion of aeration effects (via a two–phase approach) and a turbulence model. These additions will ultimately serve to establish the model as a high quality tool for use in the study of coastal engineering applications, with particular emphasis on the design of (moving) coastal structures.

Acknowledgements

We thank the reviewers for their constructive comments and suggestions on improving the quality of this paper. The financial support of University of Bath (Graduate school funding, sponsor code: 3451) and HR Wallingford (internal research project: DDY0485) for this work is greatly appreciated. All authors would like to thank Dr. Giovanni Cuomo, Research Director, HR Wallingford for his continuous support during this project. The first author gratefully thank both institutions for sponsoring his PhD study. The second author acknowledges the support of Prof. Richard Olson, Director of Extreme Events Research at Florida International University.

Appendix A. Validation of Wave Generation and Absorption in PICIN

In this Appendix we present a validation of the wave generation and absorption algorithm described in section 3. A 45 m long numerical wave tank is set up and the still water depth h is 2.5 m. A monochromatic (linear) wave with a frequency of 3.833 rad/s and wave height $H = 0.1$ m is used, which gives $h/L = 0.596$ and wave steepness $H/L = 0.024$. Computational mesh size is set to $\Delta x = \Delta z = 0.025$ m, giving 1800×110 computational cells. Note that 100 cells are initially set up to accommodate the still water, resulting in approximately 719,000 fluid particles being seeded. The Courant number used to control the variable time step is 0.5.

The waves are generated employing the wave paddle method described in section 3. The numerical prediction for the wave time–series at a distance of $3h$ from the wave maker is plotted alongside the theoretical results in Fig. A.13. It can be seen that the numerical results are in excellent agreement with the theoretical values. For the absorption boundary validation, four different damping lengths D are investigated and the results are plotted in Fig. A.14; the left panel plots the wave profile along wave tank and the right panel presents the reflection coefficient (computed by the method proposed in Goda and Suzuki (1976)) as function of the ratio between damping zone length D and wave length L. It can be seen from Fig. A.14 that the adopted relaxation damping approach works well. The reflection coefficient is around 1% for a damping

length of around 2–4 wavelengths. It is noted here that only the particle velocity is relaxed in the current PICIN model. The particle position can also be relaxed to a specified value and position. This particle position relaxation is akin to the volume fraction relaxation suggested by Jacobsen et al. (2012).

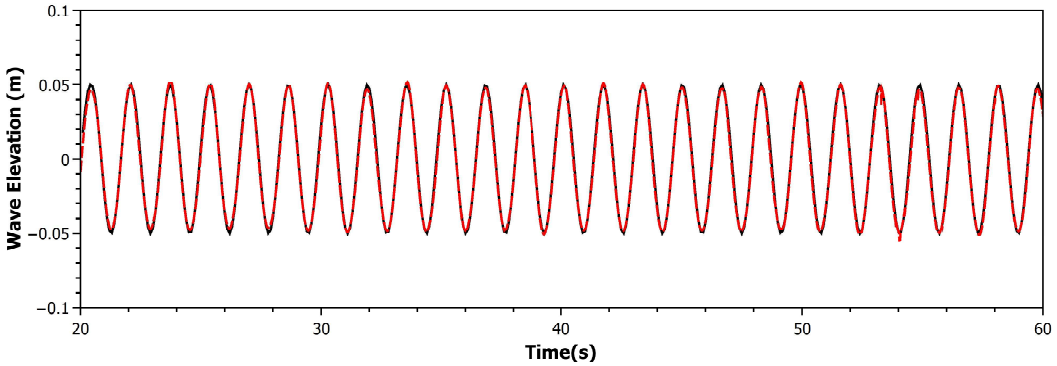

Fig. A.13: Comparison between numerical free surface time–series (dashed red line) and the theoretical results (continuous black line) at a distance $x = 3h$ from the wave maker.

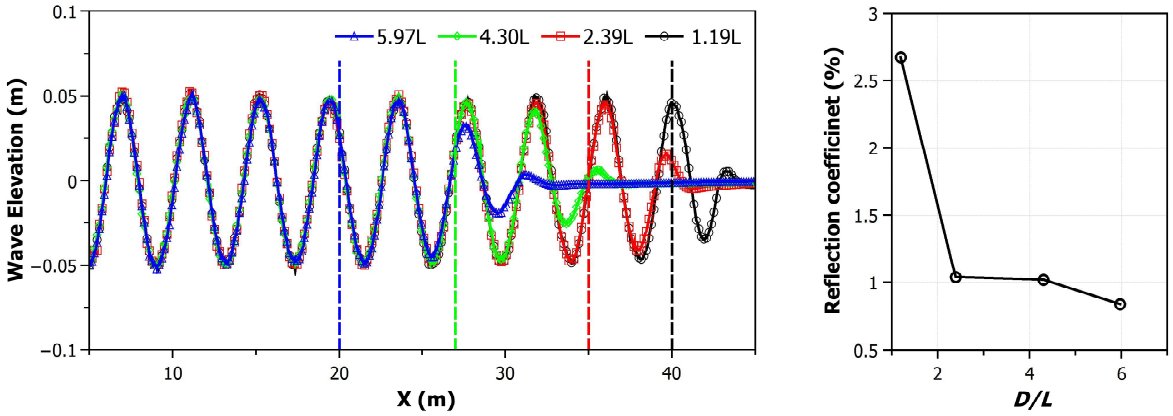

Fig. A.14: Validation results for the absorption boundary. The left panel presents wave profile along wave tank at time around $31T$, where T is the wave period; results of four different damping zone lengths D are plotted. The reflection coefficients for different damping zone lengths are given in the right panel.

References

Bouscasse, B., Colagrossi, A., Marrone, S., Antuono, M., 2013. Nonlinear water wave interaction with floating bodies in SPH. Journal of Fluids and Structures 42, 112–129.

Brackbill, J. U., Ruppel, H. M., 1986. FLIP: A method for adaptively zoned, Particle–In–Cell caluclations of fluid flows in two dimensions. J. Comp. Phys. 65, 314–343.

Chen, L., Sun, L., Zang, J., Hillis, A. J., 2014a. Numerical simulation of wave–induced roll of a 2–D rectangular barge using OpenFOAM. In: the 29th International Workshop on Water Waves and Floating Bodies. Osaka, Japan.

Chen, L., Zang, J., Hillis, A. J., Morgan, G. C. J., Plummer, A. R., 2014b. Numerical investigation of wave–structure interaction using OpenFOAM. Ocean Engineering 88, 91–109.

Chen, Q., Kelly, D. M., Spearman, J., Dimakopoulos, A., Zang, J., Williams, C. J. K., 2015a. CFD modelling of fall pipe rock dumping using PICIN. In: Proc. Coastal Sediments '15. San Diego, USA.

Chen, Q., Zang, J., Kelly, D. M., Williams, C. J. K., Dimakopoulos, A., 2015b. Particle–In–Cell numerical solver for free surface flows with fluid–solid interactions. In: 30th International Workshop on Water Waves and Floating Bodies. Bristol, UK.

Chorin, A. J., 1968. Numerical solution of the Navier–Stokes equations. Math. Comput. 22, 745–762.

Cuomo, G., Henry, A. N. W., Takahashi, S., 2010. Scaling wave impact pressures on vertical walls. Coastal Engineering 57 (4), 604–609.

Edwards, E., Bridson, R., 2012. A high–order accurate particle–in–cell method. Int. J. Numer. Methods Eng. 90 (9), 1073–1088.

Engsig-Karup, A. P., Hesthaven, J. S., Bingham, H. B., Madsen, P. A., 2006. Nodal DG-FEM solution of high–order Boussinesq–type equations. Journal of engineering mathematics 56 (3), 351–370.

Faltinsen, O. M., Landrini, M., Greco, M., 2004. Slamming in marine applications. Journal of Engineering Mathematics 48, 187–217.

Gao, F., Zang, J., 2014. Numerical simulations of breaking waves at vertical wall. In: The Eleventh ISOPE Pacific/Asia Offshore Mechanics Symposium. International Society of Offshore and Polar Engineers.

Goda, Y., Suzuki, T., 1976. Estimation of incident and reflected waves in random wave experiments. Coastal engineering proceedings 1 (15).

Greenspan, H. P., Young, R. E., 1978. Flow over a containment dyke. J. Fluid Mech.. 87(Issue 01), 179–192.

Harlow, F. H., 1964. The Particle–In–Cell computing method for fluid dynamics. In: Alder, B. (Ed.), Methods in Computational Physics. Academic Press, New York, pp. 319–343.

Harlow, F. H., Welch, J. E., 1965. Numerical calculation of time–dependent viscous incompressible flow of fluid with free surface. Physics of Fluids 8, 2182–2189.

Higuera, P., Lara, J. L., Losada, I. J., 2013a. Realistic wave generation and active wave absorption for Navier–Stokes models: Application to OpenFOAM®. Coastal Engineering 71 (0), 102–118.
URL http://www.sciencedirect.com/science/article/pii/S0378383912001354

Higuera, P., Lara, J. L., Losada, I. J., 2013b. Simulating coastal engineering processes with OpenFOAM®. Coastal Engineering 71 (0), 119–134.
URL http://www.sciencedirect.com/science/article/pii/S0378383912001093

Hirt, C. W., Amsden, A. A., Cook, J. L., 1974. An arbitrary Lagrangian–Eulerian computing method for all flow speeds. Journal of Computational Physics 14 (3), 227–253.
URL http://www.sciencedirect.com/science/article/pii/0021999174900515

Hsu, T.-J., Sakakiyama, T., Liu, P. L.-F., 2002. A numerical model for wave motions and turbulence flows in front of a composite breakwater. Coastal Engineering 46 (1), 25–50.

Jacobsen, N. G., Fuhrman, D. R., Fredsøe, J., 2012. A wave generation toolbox for the open–source CFD library: OpenFoam®. International Journal for Numerical Methods in Fluids 70 (9), 1073–1088.

Johnson, D. B., Raad, P. E., Chen, S., 1994. Simulation of impacts of fluid free surfaces with solid boundaries. International Journal for Numerical Methods in Fluids 19 (2), 153–176.
URL http://dx.doi.org/10.1002/fld.1650190205

Kelly, D. M., 2012. Full particle PIC modelling of the surf and swash zones. In: Proc. 32nd Int. Conf. Coast. Eng. A.S.C.E., Santander, pp. 77–92.
URL https://icce-ojs-tamu.tdl.org/icce/index.php/icce/article/view/6672

Kelly, D. M., Chen, Q., Zang, J., 2015. PICIN: A Particle–In–Cell solver for incompressible free surface flows with two–way fluid–solid coupling. SIAM Journal on Scientific Computing 37 (3), B403–B424.
URL http://dx.doi.org/10.1137/140976911

Koshizuka, S., Nobe, A., Oka, Y., 1998. Numerical analysis of breaking waves using the moving particle semi–implicit method. International Journal for Numerical Methods in Fluids 26 (7), 751–769.

Lin, P., Liu, P. L.-F., 1999. Internal wave maker for Navier Stokes equation models. Journal of Waterway, Port, Coastal and Ocean Engineering 125, 207–215.

Oger, G., Doring, M., Alessandrini, B., Ferrant, P., 2006. Two–dimensional SPH simulations of wedge water entries. Journal of Computational Physics 213 (2), 803–822.

Ohyama, T., Kioka, W., Tada, A., 1995. Applicability of numerical models to nonlinear dispersive waves. J. Coastal Eng. 24, 297–313.

Oliveira, T. C. A., Sánchez-Arcilla, A., Gironella, X., 2012. Simulation of wave overtopping of maritime structures in a numerical wave flume. Journal of Applied Mathematics 246146,19.

Oñate, E., Idelsohn, S. R., Celigueta, M. A., Rossi, R., 2008. Advances in the particle finite element method for the analysis of fluid–multibody interaction and bed erosion in free surface flows. Computer Methods in Applied Mechanics and Engineering 197 (19–20), 1777–1800, computational Methods in Fluid–Structure Interaction.
URL http://www.sciencedirect.com/science/article/pii/S0045782507002368

Oñate, E., Idelsohn, S. R., Del Pin, F., Aubry, R., 2004. The particle finite element method–an overview. International Journal of Computational Methods 1 (02), 267–307.

Patankar, N. A., Singh, P., Joseph, D. D., Glowinski, R., Pan, T. W., 2000. A new formulation of the distributed Lagrange multiplier/ fictitious domain method for particulate flows. Int. J. Multiphase Flow 26, 1509–1524.

Pullen, T., Allsop, N. W. H., Bruce, T., Kortenhaus, A., Schüttrumpf, H., van der Meer, J. W., 2007. EurOtop–Wave Overtopping of Sea Defences and Related Structures: Assessment Manual (Die Kuste version).
URL http://www.overtopping-manual.com/

Ramaswamy, B., 1990. Numerical simulation of unsteady viscous free surface flow. Journal of Computational Physics 90 (2), 396–430.
URL http://www.sciencedirect.com/science/article/pii/002199919090173X

Richardson, S., Cuomo, G., Dimakopoulos, A., Longo, D., 2013. Coastal structure optimisation using advanced numerical methods. In: Proceedings of Coasts, Marine Structures and Breakwaters. Edinburgh, UK.

Rogers, B. D., Dalrymple, R. A., Stansby, P. K., 2010. Simulation of caisson breakwater movement using 2–D SPH. Journal of Hydraulic Research 48, 135–141.

Ursell, F., Dean, R. G., Yu, Y. S., 1960. Forced small–amplitude water waves: a comparison of theory and experiment. Journal of Fluid Mechanics 7 (01), 33–52.

Wang, Y.-Z., Chen, N.-N., Chi, L.-H., 2006. Numerical simulation on joint motion processes of various modes of caisson breakwater under wave excitation. Comm. Num. Meth. Engng 22, 535–545.

Zhao, X., Hu, C., 2012. Numerical and experimental study on a 2–D floating body under extreme wave conditions. Applied

Ocean Research 35, 1–13.

Zhou, J. G., Stansby, P. K., 1999. An arbitrary Lagrangian–Eulerian σ (ALES) model with non–hydrostatic pressure for shallow water flows. Computer Methods in Applied Mechanics and Engineering 178 (12), 199–214.
URL http://www.sciencedirect.com/science/article/pii/S0045782599000146

Zhu, Y., Bridson, R., 2005. Animating sand as a fluid. In: Proceedings ACM SIGGRAPH. SIGGRAPH, pp. 965–972.